Science and Engineering Research Council

Rutherford Appleton Laboratory

Chilton DIDCOT Oxon OX11 0QX   RAL-92-021

New Information on Parton Distributions

A D Martin W J Stirling and R G Roberts
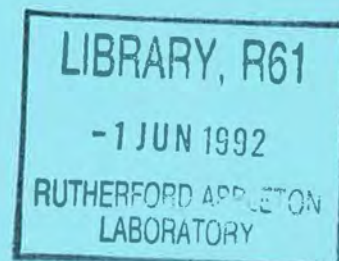
May 1992

Science and Engineering Research Council

New Information on Parton Distributions

A.D. Martin, W.J. Stirling
Department of Physics, University of Durham
Durham DH1 3LE, England

and

R.G. Roberts
Rutherford Appleton Laboratory,
Chilton, Didcot OX11 0QX, England

Abstract

New data on structure functions from deep-inelastic scattering provide new information on parton distributions, particularly in the $0.01 < x < 0.1$ interval. This has important implications for predictions for the HERA ep collider and for present and future high energy hadron colliders. We present the results of updated fits to all available precision structure function and related data. We focus in particular on two issues: (a) the increase in the sea quark distributions at small x implied by new F_2 data from the NMC collaboration, and its implications for other processes, and (b) the evidence for $SU(2)$ symmetry breaking in the light quark sea. We show that although good fits can be obtained with or without this symmetry breaking, more physically reasonable parton distributions are obtained if we allow $\bar{d} > \bar{u}$ at small x. With the inclusion of the latest deep-inelastic data we find $\alpha_s(M_Z) = 0.111^{+0.004}_{-0.005}$. We also show how W, Z and Drell-Yan production at $\bar{p}p$ colliders can give information on parton distributions.

1 Introduction

Recent determinations [1] of parton distributions have been based on analyses of precision deep-inelastic data which extend down to $x \sim 0.07$ for $Q^2 \gtrsim 5$ GeV^2. One or two measurements do exist at lower values of x, but a full range of precision data for both muon and neutrino deep-inelastic scattering on nucleons has only been available for $x \gtrsim 0.07$. As a consequence there is an increasingly wide spread in the behaviour of the different sets of parton distributions as they are extrapolated to smaller x values [2].

The behaviour of the parton distributions in the small x region, $x \lesssim 0.1$, is of considerable importance both theoretically and phenomenologically. First, the predictions of the rates of various processes which occur at the high energy hadron colliders depend on the parton densities at small x. The distributions at small x are also needed for comparison with the measurements soon to be made at the HERA ep collider. From a theoretical point of view the behaviour in the very small x region is particularly interesting since new effects are expected to emerge [3]. Indeed, one of the most important predictions of perturbative QCD is the strong increase of the gluon and sea quark distributions in the $x \to 0$ limit.

There are two main reasons why it is now timely to carry out a new (next-to-leading order) global structure function analysis and why it should yield much improved parton distributions. First, two new sets of accurate deep-inelastic data, which extend the precision measurements to smaller x values, have just become available. These are measurements of deep-inelastic scattering of muons on protons and on deuterons by the New Muon Collaboration (NMC) [4], and of neutrinos on iron nuclei by the CCFR collaboration [5]. These latter data differ significantly from the earlier CDHSW neutrino data [6]; interestingly the Q^2 behaviour predicted by the partons resulting from our previous analysis [7], which incorporated the CDHSW neutrino data, is in better agreement with the new CCFR data than with the fitted CDHSW data.

All previous global structure function analyses have assumed that $\bar{u}(x, Q^2) = \bar{d}(x, Q^2)$, that is that the light quark sea distributions are flavour independent. However, based on their F_2^n / F_2^p measurements, NMC found that [8]

$$\Sigma(0.004, 0.8) \equiv \int_{0.004}^{0.8} \frac{dx}{x} \left(F_2^p - F_2^n \right) = 0.227 \pm 0.007(\text{stat.}) \pm 0.014(\text{sys.}) \quad (1)$$

at $Q^2 = 4$ GeV^2. This is to be compared with the Gottfried sum rule [9]

$$
\begin{aligned}
I_{\text{GSR}} = \Sigma(0, 1) &\equiv \int_0^1 \frac{dx}{x} \left(F_2^p - F_2^n \right) \\
&= \frac{1}{3} \int_0^1 dx \, (u_V - d_V) + \frac{2}{3} \int_0^1 dx \left(\bar{u} - \bar{d} \right)
\end{aligned}
$$

1

$$= \frac{1}{3} \quad \text{if} \quad \bar{u} = \bar{d} \quad \text{is assumed.} \qquad (2)$$

Here $u(x, Q^2)$ has been expressed as the sum of valence and sea distributions: $u = u_V + u_S$ and $\bar{u} = u_S$, and similarly for $d(x, Q^2)$. A straightforward comparison of (1) and (2) would imply that $\bar{d} > \bar{u}$, and indeed from the lack of Regge $f - A_2$ exchange degeneracy we would expect a difference behaving as

$$(\bar{d} - \bar{u}) \propto x^{-\alpha_R} \qquad (3)$$

at small x, where the Regge intercept $\alpha_R \simeq 0.5$. Thus the second reason why it is timely to repeat the global structure function analysis is the necessity to relax the $\bar{u} = \bar{d}$ assumption and to explore the effect of incorporating a flavour breaking behaviour of the type shown in (3) in the starting sea quark distributions.

It is relevant to ask how our previous analyses [7,10] with $\bar{u} = \bar{d}$ were able to accommodate the Gottfried sum-rule measurement, or rather the precise NMC measurements of F_2^n/F_2^p at small x. We indeed found that parton distributions with $\bar{u} = \bar{d}$ can be made consistent with the NMC measurements (and all other data) provided that the u and d valence distributions have a significantly different small x behaviour. For example, the small x behaviour of the KMRS(B_0) valence partons at $Q^2 = 4$ GeV^2 is [7]

$$x(u_V + d_V) = 0.42x^{0.27}(1 + 8.1x^{0.5} + ...) \qquad (4)$$
$$xd_V = 1.49x^{0.61}(1 + 1.1x^{0.5} + ...). \qquad (5)$$

The difference in the leading x^δ-behaviour is able to give a significant contribution to $\Sigma(0, 0.004)$ to enable the Gottfried sum rule to be satisfied. Note that in the region of the data, $x \gtrsim 0.07$, the second term in (4) is dominant which leads to an effective power of x much closer to that shown in (5). Although the resulting description of the data is satisfactory we see that it is obtained at the expense of a somewhat contrived behaviour of the valence distributions at small x. Before the arrival of the new NMC and CCFR data, we had, for this reason, explored global fits which incorporated a behaviour of the type shown in (3) and found an equally acceptable description of the data, or rather a slightly improved description with a smaller number of free parameters since all the x^δ-behaviours in (3), (4) and (5) were fixed assuming that the Regge meson intercepts have $\alpha_R = 0.5$. However, instead of presenting these sets of partons, we have waited until the new data became available so as to be able to incorporate them into the analysis. We are therefore able to give a more comprehensive and much improved structure function analysis.

The paper is organized as follows. In section 2 we describe how we perform the analysis of the deep-inelastic and related data. We introduce the parametric

forms of the input x distributions, allowing for the possibility that the u and d sea quark distributions are no longer equal. Section 3 describes three different types of global fit to the data which allow (i) a comparison between a set of partons with $\bar{u} = \bar{d}$ with one with $\bar{u} \neq \bar{d}$, and (ii) a comparison between sets with singular and non-singular gluons (and sea quarks). The incorporation of the new data, particularly for $x \lesssim 0.1$, significantly modifies the distributions at small x from the values obtained in earlier analyses. In section 4 we study the consequences of the new distributions. We first discuss the effect on the Gottfried sum rule and then we investigate in some detail W, Z and Drell-Yan production. We find $p\bar{p}$ collider data for these latter processes can provide tight constraints on the parton distributions. We conclude section 4 with predictions for the behaviour of structure functions that will be measured at HERA. Finally, in section 5, we give our conclusions.

2   Fitting Procedure

The experimental measurements of the F_2 structure function for deep inelastic scattering of muon beams on hydrogen and deuterium targets have been dominated by the classic data from EMC [14] and BCDMS [12]. The considerable discrepancies between the two sets of data have, to a large extent, disappeared after adjustments of the relative normalisation and use of consistent assumptions for $R = \sigma_L/\sigma_T$. The data reached down to values of x as low as $x \approx 0.07$ for $Q^2 \gtrsim 5$ GeV^2 and this provided the final point for parton distributions to latch on to before extrapolating out into the HERA territory of really small x. In our previous analysis [7] we obtained two such sets of parton distributions, KMRS B_0 and B_-, which although giving almost identical descriptions of the data, extrapolate differently into the very small x region. These sets of partons have been widely used to predict various structure functions and hadronic cross-sections at small x and over a wide range of Q^2.

In Fig.1 we show the results of the KMRS B_0/B_- fits compared with new (preliminary) F_2 data from NMC [4]. It is clear that in the low x-region opened up by NMC (extending down to $x \approx 0.0125$) the data lie consistently *above* the old fits. In this paper we carry out a fresh analysis incorporating the new data of NMC together with new data on νN structure functions from CCFR [5] and introducing new features into the phenomenological analysis itself. As a result we produce new sets of parton distributions which reflect the new information and therefore provide a much improved basis for future phenomenology. Fig.1 also shows the result of the new fits, the improvement indicating a marked rise in the predictions at even smaller x. The comparison of the two curves emphasises how heavily the extrapolation to small x of the old distributions hung upon the BCDMS measurement at $x = 0.07$. The new data are already higher even at this x value.

3

We begin with some details of the procedure used in our next-to-leading order (NLO) QCD analysis of deep inelastic data. The parametrisation of the various parton distributions at $Q_0^2 = 4 \, \text{GeV}^2$ follows the form used in our previous analysis [7]. The gluon distribution $xg(x, Q_0^2)$ is allowed to be either finite at $x=0$ (the fits carrying a subscript 0) or singular, i.e. roughly $xg(x) \sim x^{-1/2}$ as $x \to 0$ (the subscript − being used for this case). So we write

$$xg(x, Q_0^2) = A_g \, x^{\delta_g} \, (1 + \gamma_g x) \, (1 - x)^{\eta_g} \qquad (6)$$

and, for the choices $\delta_g = 0, -\frac{1}{2}$, the parameters γ_g, η_g are determined by the prompt-photon ($pp \to \gamma x$) data of WA70 [13]. Thus in this way we shall obtain new sets of partons S_0 and D_0 (defined below) replacing KMRS [7] set B_0, and set D_- replacing KMRS set B_-.

The total sea-quark distribution at Q_0^2 is parametrised in the form

$$
\begin{aligned}
xS &\equiv 2x \, (\bar{u} + \bar{d} + \bar{s}) \\
&= A_S \, x^{\delta_g} \, (1 + \epsilon_S x^{1/2} + \gamma_S x) \, (1 - x)^{\eta_S} \qquad (7)
\end{aligned}
$$

reflecting the fact that the sea-quarks are expected to have the same leading $x \to 0$ behaviour as the gluon. The charm quark distributions are generated, as usual, through the evolution equations taking $c(x, Q_0^2) = 0$. The strange sea is known to be roughly half the $\bar{u}$ or $\bar{d}$ sea so we take $\bar{s} = \frac{1}{4}(\bar{u} + \bar{d})$, at Q_0^2. As discussed in the introduction a new feature of the analysis is the freedom for the $\bar{u}$ and $\bar{d}$ distributions to differ. The parametrisations of the sea quark distributions at Q_0^2 are therefore written as

$$
\begin{aligned}
2\bar{s} &= 0.2 \, S \\
2\bar{d} &= 0.4 \, S + \Delta \\
2\bar{u} &= 0.4 \, S - \Delta \qquad (8)
\end{aligned}
$$

with

$$
\begin{aligned}
x\Delta &\equiv x \, (\bar{d} - \bar{u}) \\
&= A_\Delta \, x^{\eta_\Delta} \, (1 - x)^{\eta_S}. \qquad (9)
\end{aligned}
$$

The value of the Gottfried sum rule (2) is then given by

$$I_{GSR} = \frac{1}{3} - \frac{2}{3} \, A_\Delta B(\eta_\Delta, 1 + \eta_S). \qquad (10)$$

We actually carry out fits with $A_\Delta = 0$ (labelled as S for $\bar{u}$ and $\bar{d}$ the *same*) and with $A_\Delta \neq 0$ (labelled as D for $\bar{u}$ and $\bar{d}$ *different*). We can thus study the effect of

allowing $\bar{u} \neq \bar{d}$ by comparing fit S_0 with fit D_0, and study the effects of a singular gluon by comparing fit D_0 with fit D_-.

The distribution $\Delta(x)$ is thus a flavour non-singlet and we would expect, by Regge behaviour, $\eta_\Delta \approx \frac{1}{2}$. The other non-singlet distributions are the valence quarks parametrised by

$$x[u_V(x) + d_V(x)] = A_{ud} \, x^{\eta_1} \, (1-x)^{\eta_2} \, (1 + \epsilon_{ud} x^{1/2} + \gamma_{ud} x)$$
$$x d_V = A_d \, x^{\eta_3} \, (1-x)^{\eta_4} \, (1 + \epsilon_d x^{1/2} + \gamma_d x) \qquad (11)$$

with A_{ud} and A_d fixed in terms of the η's, ϵ's and γ's to give the correct number of valence quarks.

As is well known, the singular gluon ($\delta_g = -\frac{1}{2}$), as x decreases, ultimately leads to significant gluon-gluon interactions which "soften" this behaviour. These shadowing effects are the centre of intense study and will be one of the major subjects of investigation at HERA. We follow precisely the same procedure detailed in KMRS [7] and introduce two types of modification to take account of this gluon-recombination. Firstly the small x behaviour of the gluon distribution (and the sea distribution) is altered at Q_0^2,

$$xg(x, Q_0^2) \to xg(x, Q_0^2) \left\{ 1 + \frac{\theta(x_0 - x)[C(x)x^{-1/2} - C(x_0)x_0^{-1/2}]}{xg_{\rm sat}(x, Q_0^2)} \right\}^{-1} \qquad (12)$$

where the unmodified distribution $xg(x) \sim C(x)x^{-1/2}$, and where

$$xg_{\rm sat}(x, Q^2) = 16R^2 Q^2 / 27\pi\alpha_s(Q^2) \qquad (13)$$

is the value of the gluon which would saturate the unitarity limit. The form of eq.(12), which leads to shadowing corrections only for $x < x_0$, is justified in ref.[7]. Shadowing effects are important only for very small x and we find it reasonable to choose $x_0 = 10^{-2}$. Thus it is sufficient and convenient to impose the corrections after fitting to the data which all lie in the region $x > x_0 = 10^{-2}$. As in [7] we consider two values of the radius parameter R which characterises the nature of the coupling of the gluon ladder to the proton or, to put it another way, which describes how the gluons are distributed within the proton. We take $R = 5$ GeV^{-1} ($\sim$ proton radius), which corresponds to the gluons being uniformly spread throughout the proton and then repeat the calculation with $R = 2$ GeV^{-1} to illustrate the effect of concentrating the gluons in "hot-spots" within the proton. This latter picture represents a rather extreme limit of the shadowing mechanism - in practise it leads to a suppression of the singular gluon to the extent that it is then not far from the finite gluon solution ($\delta_g = 0$). The second modification due to shadowing is in the

5

evolution of the gluon and sea distributions. A non-linear term is incorporated into the evolution equations whose size is governed by the shadowing radius,

$$\frac{\partial(xg(x,q^2))}{\partial \ln Q^2} \to \frac{\partial(xg(x,q^2))}{\partial \ln Q^2} - \frac{81\alpha_s^2(Q^2)}{16R^2Q^2} \int_x^{x_0} \frac{dx'}{x'} [x'g(x',Q^2)]^2 \qquad (14)$$

and an analogous, but more complicated, modification for the evolution of the sea quark. The details are to be found in ref.[7]. Again the modifications are relevant only for $x < x_0$. However the suppression it causes for $x < x_0$ will lead to a small violation of the momentum sum rule, which we restore by a simple renormalisation of the distributions.

The deep inelastic data that are used in the global analysis are:

(i) the new, but preliminary, NMC data on $F_2^{\mu p}$ and $F_2^{\mu D}$ [4]

(ii) BCDMS data on $F_2^{\mu p}$ and $F_2^{\mu D}$ [12]

(iii) data on $F_2^{\mu n}/F_2^{\mu p}$ from NMC [15], BCDMS [16], EMC [17]

(iv) the wide-band beam neutrino data from CCFR [5] and CDHSW [6] on $F_2^{\nu N}$ and $xF_3^{\nu N}$

In addition to these deep-inelastic data we also incorporate

(v) WA70 data on prompt photon production [13]

(vi) E605 data on Drell-Yan production [18]

(vii) constraints from W and Z production at $p\bar{p}$ colliders (see section 4.3).

The new input in (iv) are the preliminary wide-band beam neutrino data from CCFR which show a significant deviation from the CDHSW wide-band beam data. As in our previous analyses which include data taken from experiments using heavy nuclear targets, we correct for the nuclear distortion to the structure functions. The correction is based on precise measurements of the ratio of iron to deuterium cross sections. In addition to the parameters describing the starting parton distributions in eqs.(6 - 11) we also have $\Lambda_{\overline{MS}}$ and the relative normalisations of the data sets. When compared with the SLAC data [19], the BCDMS data required a 2% shift down (whereas the EMC data needed to be shifted up by $\sim 7\%$). We find, as a result of our new fits, that this shift remains for the BCDMS relative to the NMC. We find that a larger shift is required for the CCFR data. In summary, relative to the SLAC data, the renormalisations of the BCDMS, NMC, CDHSW and CCFR data sets are found to be 0.98, 1.00, 1.00 and 0.94 respectively. More accurate renormalisations must await the final experimental analyses.

6

3 Fits to Data

As mentioned above, we perform three different types of fit to the data to explore first the effect of allowing $\bar{u}$ to be different from $\bar{d}$ and, second, the difference between starting the evolution with a singular and non-singular gluon. The resulting three sets of partons are labelled :-

(i) S_0 : $xg(x, Q_0^2) \sim$ constant as $x \to 0$, and $\bar{u} = \bar{d}$

(ii) D_0 : $xg(x, Q_0^2) \sim$ constant as $x \to 0$, and $\bar{u} < \bar{d}$

(iii) D_- : $xg(x, Q_0^2) \sim x^{-1/2}$ as $x \to 0$, and $\bar{u} < \bar{d}$

We also study the effect of shadowing on the small x behaviour of the D_- distributions, according to eqs.(12-14) with both $R = 5$ GeV^{-1} and 2 GeV^{-1}.

The values of the parameters obtained in the three fits are listed in Table 1. All three resulted in a value of Λ of QCD

$$\Lambda_{\overline{MS}}(n_f = 4) = 215 \pm 60 \text{ MeV} \tag{15}$$

where the error includes the uncertainty due to scale dependence [20]. This corresponds to

$$\alpha_s(M_Z) = 0.111^{+0.004}_{-0.005}. \tag{16}$$

The inclusion of the new data has thus slightly raised the prediction for the strong coupling from our previous value [20] of

$$\Lambda_{\overline{MS}}(n_f = 4) = 190 \pm 80 \text{ MeV} \quad \text{or} \quad \alpha_s(M_Z) = 0.109^{+0.007}_{-0.008} \tag{17}$$

The value of the strong coupling, shown in (15) or (16), is in excellent agreement with an independent determination [21] using a BCDMS and SLAC subset of the deep inelastic data. It is also in agreement with the determination from the LEP experiments [22] based on event topology :

$$\alpha_s(M_Z) = 0.120 \pm 0.007. \tag{18}$$

Indeed the accuracy of the deep inelastic determination of $\alpha_s(M_Z)$ is comparable to that presently available at LEP.

The values of the x exponents of the valence quarks in the S_0 fit, $\eta_1 = 0.26$ and $\eta_3 = 0.78$, contrive to make $x(u_V - d_V)$ fall slowly as $x \to 0$ and so be consistent with NMC data on $F_2^p - F_2^n$ as well as the $\frac{1}{3}$ value of the integral $I_{\text{GSR}} \equiv \Sigma(0, 1)$ of eq.(2). In the D type fits, the value of η_Δ always came close to $\frac{1}{2}$ as expected.

7

Now we turn to the resulting comparison with the data. Fig.2 shows the new NMC (preliminary) and the BCDMS data ($\times$ 0.98) for $F_2^{\mu p}$. It is clear that we have obtained a fit which is able to describe the new data while still maintaining success in fitting the larger x region of the BCDMS data. The same is true for the deuterium data shown in Fig.3. The dashed curves in Fig.2(a) show that the predictions of the KMRS partons [7], extrapolated from fits to the BCDMS data with $x \gtrsim 0.07$, considerably undershoot the new $F_2^{\mu p}$ data at smaller x. The situation is also well illustrated by Fig.1.

In Fig.4 the data on $F_2^{\mu n}/F_2^{\mu p}$ from NMC are compared with the three fits. Although EMC and BCDMS data are also included in the fits, it is the very precise NMC data which tend to drive the resulting parameters. The S_0 fit, like the old B_0 fit of KMRS, needs to juggle with the exponents η_1 and η_3, which govern the small x region of the valence quarks, in order to agree with the very small x points. In contrast, the extra freedom of having $\bar{u} \neq \bar{d}$ allows the parameters η_1, η_3 and η_Δ to be all different but the fits prefer to have all three values close to $\frac{1}{2}$. The extraction of the n/p ratio from experiment requires a nuclear correction for the deuteron and since the binding is weak this correction, certainly at small x, is bound to be small. However at small x, our fits are sensitive to the small quantity $\rho = [1 - F_2^{\mu n}/F_2^{\mu p}]$ which is just $2[1 - F_2^{\mu D}/F_2^{\mu p}]$ where $D \equiv \frac{1}{2}(p + n)$. A small fractional charge δ to D leads to an absolute change -2δ to ρ and so any uncertainty in the deuteron correction at small x implies significant uncertainty in the parameters describing the small x behaviour.

Figs.5 and 6 show the new (preliminary) νN data on F_2 and xF_3 from CCFR [5] compared with the CDHSW data [6] (also obtained using a wide band neutrino beam). The continuous curves are our fit to the new CCFR data. The renormalisation of the CCFR data by 6% relative to the CDHSW data is important in obtaining acceptable fits. The dashed curves in Figs.5 and 6 show, for comparison, the KMRS fits obtained in an earlier global analysis [7] which included only the neutrino data of CDHSW. One can see the improved quality of the new fit, even with the CDHSW data alone.

A summary of the quality of the description of the deep inelastic data by each of the three sets of partons is given in Table 2. There we tabulate the contribution to the total χ^2 arising from the individual subsets of data.

Fig.7 shows our description of the WA70 [13] prompt photon production data, $pp \to \gamma X$. Here the dominant QCD subprocess is $qg \to \gamma q$ and these data pin down the gluon distribution in the region $x \sim 0.4$.

8

4 Implications and Consequences

The continuous curves in Fig.8 show the D_0 set of parton distributions as a function of x at $Q^2 = 20$ GeV^2. For comparison we also show the distributions of the B_0 set obtained in the earlier KMRS analysis. Though the agreement is excellent for $x \gtrsim 0.1$, we see the quark distributions differ significantly at small x, reflecting the influence of the new small x data. Likewise the quark distributions of solutions S_0 and D_- are also considerably above those of the B_0 set at small x. In this section we explore the consequences of the new solutions and discuss future measurements which may be able to distinguish between the differing small x behaviours. We begin by looking again at the Gottfried sum rule.

4.1 Gottfried sum rule

As discussed in section 1, one of the motivations for relaxing the $\bar{u} = \bar{d}$ assumption of our previous fits was to better accommodate the lower value of the Gottfried sum rule indicated by the NMC measurement [8]. Although fits with $\bar{u} = \bar{d}$ could successfully describe the integrand $F_2^{p-n} \equiv F_2^p - F_2^n$ [10] the exponents η_1, η_3 are found to have rather unphysical values. However there is no strong theoretical justification for maintaining the equality $\bar{u} = \bar{d}$. Indeed, as mentioned in sections 2 and 3, choosing $\bar{u} \neq \bar{d}$ results in a more "natural" situation where the values of the exponents η_1, η_3, and η_Δ all cluster around the Regge expectation of $\frac{1}{2}$. In Fig.9 we show the values of F_2^{p-n} from our fits at $Q^2 = 7$ GeV^2. As expected, the D-type fits drop significantly faster at small x than the S_0 fit. The experimental estimates of the difference $F_2^p - F_2^n$ and of the sum rule published by NMC [8] were based on combining their own measurements of the n/p ratio with a fit to F_2^D from other experiments,

$$F_2^{p-n}(x) = 2 F_2^D(x) \frac{1 - F_2^n/F_2^p}{1 + F_2^n/F_2^p}. \tag{19}$$

This fit does not reflect the new information at small x and a more recent, but preliminary, estimate from NMC [4], obtained directly from their new structure functions is shown by the data points in Fig.9.

Also shown in Fig.9 are the resulting estimates of the integral

$$\Sigma(0, x) = \int_x^1 \frac{dx'}{x'} F_2^{p-n}(x'). \tag{20}$$

At $x = 10^{-3}$ all three fits give values around 0.26-0.27 though the "asymptotic" values for the S and D type fits are quite different (see Table 1). It is hard to say

precisely how the experimental estimate of the Gottfried sum rule will be modified as a result of the new data at small x. A recent study [24] of possible nuclear corrections to F_2^D demonstrated that changes of the order of 3% to F_2^D could lead to changes in the value of $\Sigma(0,1)$ by nearly 40%. On the other hand explicit estimates [25] of shadowing corrections to deuterium indicate effects well under 2% in the range of the NMC data.

In Fig.10 we show the resulting u and d sea-quark distributions and their difference at two widely different values of Q^2. The difference $x\Delta(x)$ reaches its peak around $x = 0.04$. The value of $x\bar{u} = x\bar{d}$ for the S_0 fit is sandwiched between the values of $x\bar{u}$ and $x\bar{d}$ for the D_0 fit.

4.2 Q^2 dependence of structure functions

One of the interesting new pieces of information in this analysis is the new (preliminary) set of wide band neutrino data from CCFR [5]. Perhaps the most significant feature is the difference in the Q^2 behaviour of the two data sets. The discrepancy may not be immediately obvious from Fig.5 but if we compute the derivative $d\log F_2(x, Q^2)/d\log Q^2$ at fixed x values the difference becomes plain to see. Fig.11 shows the values of this derivative for each data set compared with the resulting QCD prediction of this analysis. It is clear that the new data are more in line with the expectations of the theory. It is most important in making such a comparison that only data on the structure functions which fall in the range of validity of leading twist QCD, namely $Q^2 > 5$ GeV^2 *and* $W^2 > 10$ GeV^2, are used in computing the experimental values of the derivative. For example, removing the W^2 cut modifies the large x points substantially. When the full CCFR data becomes available it will be interesting to see if the consistency with QCD continues out to large x. Such consistency is graphically demonstrated for the muon data in Fig.12 where the small uncertainties in the BCDMS values of F_2 allow a very precise determination of the derivatives. Again, these derivatives are computed from data satisfying the required cuts in Q^2 and W^2. Because of these cuts the error on the NMC point at $x = 0.5$ becomes very large.

4.3 W, Z and Drell-Yan hadroproduction

One of the most direct tests of parton distributions comes from "Drell-Yan" type processes: $q\bar{q} \rightarrow W, Z, \gamma^*(\rightarrow l^+l^-)$. In fact we have already used the fixed target Drell-Yan dilepton data from E605 to constrain the sea distribution at medium to large x values. At the $p\bar{p}$ colliders, on the other hand, the higher collision energies provide a probe of the quarks and antiquarks at smaller x values. In addition the dominant contributions to the cross sections come from the scattering of essentially

10

the same "valence + sea" combinations that enter in the deep inelastic scattering structure functions.

Since our main interest in the present study is the new information on the quark distributions in the $0.01 - 0.1$ x range, we address the question of whether W, Z or Drell-Yan (*i.e.* dilepton) cross sections measured in $p\bar{p}$ collisions at $\sqrt{s} = 630$ GeV and 1.8 TeV can provide independent information on the quark distributions. In what follows we will compare the predictions of the old and new sets for various electroweak cross sections measured at the $p\bar{p}$ colliders. It will prove useful in understanding the differences between the predictions to refer back to the differences in the quark distributions themselves, illustrated in Fig.8.

We can summarize the relevant collider phenomenology as follows:

(i) The *total cross section* $\sigma_W \equiv \sigma(p\bar{p} \rightarrow W + X)$ is sensitive to the u and d distributions around $x \sim M_W/\sqrt{s}$.

(ii) The *ratio of W to Z total cross sections* $R_\sigma \equiv \sigma_W/\sigma_Z$ is sensitive to the magnitude of the ratio of d and u quarks, just like the structure function ratio $F_2^{\mu n}/F_2^{\mu p}$.

(iii) The *$W \rightarrow$ charged lepton rapidity asymmetry*

$$A(y) = \frac{d\sigma(l^+)/dy - d\sigma(l^-)/dy}{d\sigma(l^+)/dy + d\sigma(l^-)/dy} \tag{21}$$

is also sensitive to the d/u ratio, but more to the slope in x rather than the absolute magnitude [26].

(iv) The *Z rapidity distribution* at large y_Z probes the quark distributions at much smaller $x \sim \exp(-y_Z)M_Z/\sqrt{s}$ than the total cross section.

(v) The *lepton-pair cross section* $M^3 d\sigma/dMdy|_{y=0}$, where $M = M_{l^+l^-}$ and $y = y_{l^+l^-}$, is also sensitive to the (dominantly u) quark distributions, and since the $p\bar{p}$ collider experiments can in principle measure dimuon masses down to $M = M_\Upsilon \sim 10$ GeV, this means significantly smaller x values than are probed by σ_W or σ_Z.

Figs.13-18 and Table 3 show the predictions of the new parton sets S_0, D_0 and D_- for all the above quantities, together with the measurements from the $p\bar{p}$ collider experiments where available. For comparison, the predictions of the previous B_0 set are also shown.

Fig.13 shows the total W and Z production cross sections times leptonic branching ratios as a function of the $p\bar{p}$ collider energy $\sqrt{s}$, together with recent measurements from the UA2 [27] and CDF [28] collaborations. The theoretical predictions

11

are calculated to $O(\alpha_s^2)$ in QCD perturbation theory, using the results of Hamberg *et al.* [29]. The renormalisation and factorisation scales are set equal to the weak boson masses: $Q = \mu = M_V$, with $M_W = 80.14$ GeV [30] and $M_Z = 91.175$ GeV [31]. Values for the branching ratios

$$B(W \to e\nu) = 0.108, \quad B(Z \to e^+e^-) = 0.0336 , \tag{22}$$

corresponding to three light neutrinos and $m_t > M_W$, are used. At 630 GeV the predictions are very similar, simply because at this value of $x \sim M_W/\sqrt{s} \sim 0.13$ all the sets are constrained by the same structure function data, dominantly the $F_2^{\mu p}$ data from BCDMS and the n/p ratio from NMC. At 1800 GeV $(M_W/\sqrt{s} \sim 0.04)$ we begin to see the effect of the new NMC F_2 data: the predictions of the new sets are now significantly above the previous B_0 prediction. This increase can be directly related to the behaviour of the B_0 and D_0 quark distributions shown in Fig.8. Unfortunately the CDF data are not yet precise enough to discriminate between the old and new predictions. Note that our predictions are all slightly higher than the UA2 cross section measurements. We have investigated whether the quark distributions can be adjusted to improve the agreement, but we find that the deep inelastic structure function data do not permit the $O(5\%)$ decrease in the quark distributions which would be required. In view of the non-negligible experimental errors and theoretical uncertainties in the calculation, we do not regard the small disagreement as significant. Note that the *ratio* of the W and Z cross sections is better described, indicating consistency with the n/p structure function ratio. The experimental measurements and the theoretical predictions at $\sqrt{s} = 630$ GeV and 1800 GeV are summarised in Table 3. Fig.14 shows the predictions extended to higher collision energies. The main feature is the steeper increase of the cross sections for the D_ set, driven mainly by the more singular $x^{-3/2}$ small-x behaviour of the sea quark distributions. We emphasize that the spread of the predictions at LHC and SSC energies arises simply from our assumptions about the small-x behaviour of the parton distributions, and should not therefore be taken as indicative of the overall theoretical uncertainty. Only when HERA begins to provide information on the structure functions at small x will the predictions become more precise.

Because the u and d quark distributions in the proton are different, W^+ (W^-) bosons are produced preferentially in the direction of the incoming proton (antiproton) in $p\bar{p}$ collisions. A measurement of the $W^\pm$ rapidity *asymmetry* therefore provides information of the d/u ratio of quark distributions. Fig.15 shows the W^+ rapidity distribution at $\sqrt{s} = 1.8$ TeV obtained from the S_0, D_0 and D_ sets of partons, together with the previous B_0 prediction for comparison. The curves are calculated in $O(\alpha_s)$ perturbative QCD; the second order corrections are not yet

known for the rapidity distribution. Evidently, the rapidity asymmetry for all the sets is similar: the asymmetries for S_0 and D_0 are almost identical, and lie between those of sets B_0 and D_-. What is measured in practice is of course the *charged lepton* rapidity asymmetry, defined above. In principle this carries as much information about the quark distributions as the W rapidity asymmetry, since the $W \to l\nu$ decay is completely known. Fig.16 shows the predictions of the four sets for the lepton rapidity asymmetry, together with data from the CDF collaboration [33]. The calculations are performed in leading order, with the same transverse mass cuts as used in the experiment.(The $O(\alpha_s)$ correction to the asymmetry has recently been calculated [34] and shown to reduce the leading order asymmetry slightly.) Note that the highest y data point has a higher transverse mass cut, hence the discontinuity in the predictions. Overall the agreement is very satisfactory, with the new sets slightly favoured. The fact that all sets give similar asymmetries can again be traced back to the fact that they are all fitted to the same n/p structure function ratio data. In reference [26] it was shown that the size of the asymmetry was strongly correlated with the magnitude of the *slope* of the n/p ratio in the relevant x region. In fact, the new sets have a slightly larger n/p slope than the previous B_0 fit – compare Fig.4 with Fig.7 of reference [7] – and therefore the aysmmetry is correspondingly slightly larger.

With the prospect of a substantial increase in integrated luminosity at the Fermilab $p\bar{p}$ collider in the next few years, it should be possible to obtain further information on the small x quarks from the shape of the Z *rapidity* distribution, which can in principle be reconstructed from the lepton four-momenta. We have already seen how the *total* cross section is indeed slightly larger at 1.8 TeV for the new sets, reflecting the larger quark distributions around $x \sim M_Z/\sqrt{s}$. This integrated cross section is dominated by Z's produced with small rapidity. At larger rapidity, one of the incoming partons is forced to smaller x:

$$x_{1,2} \sim \exp(\pm y_Z) \, \frac{M_Z}{\sqrt{s}} \, , \tag{23}$$

and we would expect the differences between the predictions based on the old and new sets to be enhanced. This is illustrated in Fig.17, where the curves are labelled as before. (Note that the rapidity distribution is symmetric about $y_Z = 0$.) The effect is seen at large y_Z: the new distributions produce broader Z rapidity distributions: S_0 and D_0 are broader than B_0, and D_- is broader still. If there is sufficient acceptance for leptons at large rapidity, then the only issue in practice is one of statistics. Note that an integrated luminosity of 20 pb^{-1}yr^{-1} corresponds to $O(8000)$ dilepton (e, μ) events per year at $\sqrt{s} = 1.8$ TeV which, even allowing for efficiency losses, should be sufficient for a significant discrimination. At even higher collider energies the differences between the more singular D_--type and the

13

standard D_0-type distributions become apparent. For example, it was shown in reference [35] that at LHC and SSC energies, the singular D_--type distributions give Z rapidity distributions which actually have maxima at large y_Z, rather than at $y_Z = 0$.

Fig.18 shows the Drell-Yan cross section $M^3 d\sigma/dMdy$ at $y = 0$ for the two collider energies, as a function of the dilepton mass M. The labelling of the curves is the same as in the previous figures. The difference between the old and new distributions is clearly seen as an enhancement of the cross sections at small mass for the latter: being proportional to the square of the parton distributions, the Drell-Yan cross section amplifies the differences between the old and new quark distributions in the $0.01 - 0.1$ x range, Fig.8. At larger dilepton masses, the predictions come together as larger x values are probed.

Also shown in Fig.18(a) are recent data from the UA1 collaboration [36]. The errors are statistical only and there is an additional overall systematic error estimated at 14% [37]. Although it is tempting to conclude that they favour the new distributions, it must be remembered that the predictions are calculated to $O(\alpha_s)$ only – the second order corrections for distributions differential in mass *and* rapidity are not yet known. Note that if we use as a guide the correction to the total (*i.e.* rapidity integrated) cross section [29], we might expect a small negative second-order correction to the differential distribution. In view of the importance of these Drell-Yan data in providing independent information on the quarks at small x, we regard the calculation of the $O(\alpha_s^2)$ corrections to the differential distribution as a matter of some urgency. At the higher collider energy, Fig.18(b), the differences between the old and new sets are even larger, and we also begin to see, at small dilepton masses, the appearance of the more singular small-x behaviour of the D_- distributions. An accurate measurement of the Drell-Yan cross section in this mass range at $\sqrt{s} = 1.8$ TeV would be extremely useful.

4.4   Predictions for HERA

Clearly the impact of the new information that has been included in this analysis is on the physics of the small x region. Since HERA is designed to explore the region $x/Q^2 \gtrsim 10^{-5}$ GeV^{-2}, it is important to predict as reliably as possible the consequences of different theoretical models in order for the experimental measurements to differentiate between them. Compared to our previous analysis [7], not only are the extrapolations to $x < 0.01$ significantly different – their reliability is much improved.

Fig.19 shows how F_2 is expected to behave at low x as a result of the parton distributions shown in Fig.8. The dramatic change in the quark distributions

compared to those of B_0 is reflected in expectations for F_2 at $x \approx 10^{-4}$ which are 50-80% higher than the corresponding curves in Fig.12 of ref.[7]. HERA probes the kinematic region in which shadowing corrections suppress the effects of the singular behaviour of the gluon and sea quark distributions of the D_- type of solution. The $D_-(R = 5)$ curve in Fig.19 shows the effect of conventional shadowing for which we assume the partons are uniformly spread throughout the proton with radius $R = 5$ GeV^{-1}. The effects of the more extreme form of shadowing, in which it is assumed that the partons are concentrated in "hot spots", are shown by the $D_-(R = 2)$ curve. Given the precision with which HERA eventually expects to measure F_2 there is a reasonable chance of distinguishing between the various assumptions for the behaviour of partons. Fig.20 shows the expectations at other values of Q^2 including the ranges of x and Q^2 which can be probed by ep collisions at LHC.

As emphasized before, the measurement of the longitudinal structure function F_L at small x, although more difficult than that of F_2, is much more sensitive to the nature of the gluon. Fig.21 illustrates the intimate connection between F_L and xg at small x which can be exploited to extract a much more precise estimate of the gluon distribution [38]. For completeness, we note that inelastic J/ψ production at HERA has also been advocated [39] as a promising measurement of the small x behaviour of the gluon. A recent comprehensive review of J/ψ production has been given by Jung et $al.$ [40].

Perturbative QCD predicts [41] a singular $x^{-\lambda}$ behaviour of the gluon and sea quark distributions, as typified by our D_- set of partons. Indeed this small x behaviour is characteristic of the leading $\log(1/x)$ summation of multiple soft gluon emissions. However, as we have seen, no experimental data yet exist to distinguish this so-called "Lipatov" behaviour from the more traditional small-x behaviour of the D_0 and S_0 sets. Although measurements of F_2, F_L and J/ψ at HERA should be able to probe the relevant small x region, it has been advocated [42] that the "Lipatov" $x^{-\lambda}$ behaviour can be more cleanly identified by observing small-x deep-inelastic events which contain a measured jet. The application of this method [43] at HERA will rely on the parton distributions being reliably known for $x \gtrsim 0.01$, but not at smaller x.

5   Conclusions

There are several reasons why it is important to have parton distributions which are as accurate as possible. First, the very fact that it is possible to extract a $consistent$ set from the growing amount of high-precision data covering a wide number of different processes is itself an impressive acknowledgement of the validity of the un-

derlying theory. Second, the improvement in precision of the parton distributions allows increasingly reliable estimates to be made for processes in new kinematic ranges, in particular at higher energies. The 'MRS philosophy' is to continually update and improve the parton distributions as new experimental information becomes available. This program is complementary to the advances in the calculation of even higher order perturbative QCD corrections.

Recent deep inelastic scattering data from NMC [4] have shed new light on the region $0.01 < x < 0.1$, as well as confirming existing measurements at larger x. These new data lead to an increase in previous estimates of the parton distributions (based largely on extrapolation) below $x \sim 0.05$, and also appear to confirm the previous result that the value of the Gottfried sum rule is most likely less than the contribution from valence quarks alone. The natural way to accommodate this result is to relax the $\bar{u} = \bar{d}$ constraint assumed in all previous parton distribution analyses. In the present study we provide parton distributions with or without the $\bar{u} = \bar{d}$ constraint (S or D type) and show that the D type is indeed a more natural choice. It would be interesting to find an independent phenomenological preference for either S or D solutions. This seems to be hard − for example the $\bar{p}p \to W, Z$ cross sections, being largely dominated by valence-valence collisions, are quite insensitive to the choice. The most promising route, which we will address in a future study, appears to be in comparing Drell-Yan production in pp and pn collisions [44].

There are new data also on neutrino deep inelastic scattering from the CCFR collaboration which we have included. Consistency with other deep inelastic data is achieved if the CCFR data are shifted down by 6%, but more significantly these new data show a vastly improved agreement with the Q^2 behaviour expected from perturbative QCD.

We stress the importance of examining *all* processes that involve the parton distributions. We have considered several cases where there are direct connections between features of deep inelastic scattering and of hadronic reactions. For example, the *ratio* of the W and Z cross sections in $\bar{p}p$ collisions is tied to the *ratio* n/p of the structure functions at $x \sim M_V/\sqrt{s}$, while the *asymmetry* of the $W^\pm$ rapidity distributions is governed by the *slope* of the n/p ratio at that x value. The *magnitude* of the W cross section is rigidly constrained by the *size* of F_2 at $x \sim M_W/\sqrt{s}$ and so the cross sections at the CERN SPS collider are already tightly constrained by the previous structure function measurements at $x \sim 0.13$, while those at the Fermilab collider are influenced by the new NMC measurement of F_2 around $x \sim 0.04$. Likewise, in the future predictions at LHC/SSC will be based on structure function measurements at HERA in the region $x \sim 0.005$.

Of course we can already make predictions for the very small x region based

16

on extrapolations of our fits, but the major uncertainty arises from the assumed behaviour of the gluon and sea quark distributions. As a measure of this uncertainty we provide two possible sets of partons, one (D_0) based on "finite" gluons and sea quarks as $x \to 0$ and the other (D_-) based on singular forms $\sim x^{-\lambda}$ which have theoretical justification based on resumming soft gluon emissions.[1] However this "Lipatov" gluon is almost certainly softened by some shadowing correction the size of which, in turn, is a matter of debate. We have therefore provided another two parton sets which choose either a conventional shadowing correction (with radius $R = 5$ GeV^{-1}) or one corresponding to the "hot spot" scenario (with radius $R = 2$ GeV^{-1}). One of the aims of this analysis is to suggest phenomenological "pointers" which will hopefully reveal the gluon's nature. We have studied the consequences of the different solutions for measurements of F_2 and F_L at HERA, and the indications are that the latter – together with the measurement of J/ψ production – will reveal the correct small-x behaviour. But in the long term it will be the high-energy proton-proton colliders which will provide quantitative tests of the really small x behaviour – again, W and Z production will be an important tool.

Finally, while we have concentrated on the impact of new experimental information on the small x region, we should emphasize that there has been little change in the situation at $x > 0.1$ (see Fig.8). Our previous analyses [45] of processes like top quark and large p_T jet production in high-energy $p\bar{p}$ collisions, which are not sensitive to the small-x region, are still valid.

Acknowledgements

---

[1]The distributions S_0, D_0, D_- as well as the old B_0 can be obtained by electronic mail from WJS @ UK.AC.DUR.HEP or DURHEP::WJS

17

References

[1] P.N. Harriman, A.D. Martin, R.G. Roberts and W.J. Stirling, Phys. Rev. **D42** (1990) 798.
J. Kwiecinski, A.D. Martin, R.G. Roberts and W.J. Stirling, Phys. Rev. **D42** (1990) 3645.
J. Morfin and W.K. Tung, Zeit. Phys. **C52** (1991) 13.
M. Diemoz, F. Ferroni, E. Longo and G. Martinelli, Zeit. Phys. **C39** (1988) 21.

[2] See for example: H. Plothow-Besch, Proc. 3rd Workshop on Detector and Event Simulation in High Energy Physics, Amsterdam, April 1991.

[3] Recent reviews are
B. Badelek, K. Charchula, M. Krawczyk and J. Kwiecinski, preprint DESY 91-124.
E. M. Levin, preprint DESY 91-110.

[4] NMC collaboration: M.W. van der Heijden, University of Amsterdam thesis, 1991.
E. Kabuß,invited talk at DESY-Zeuthen Workshop on Deep Inelastic Scattering, April 1992.

[5] CCFR collaboration: S.R. Mishra presentation of preliminary wide band beam data at Lepton-Photon Symposium, Geneva 1991.

[6] CDHSW collaboration: J.P. Berge *et al.*, Zeit. Phys. **C49** (1990) 187.

[7] J. Kwiecinski, A.D. Martin, R.G. Roberts and W.J. Stirling, Phys. Rev. **D42** (1990) 3645 (abbreviated KMRS).

[8] NMC: P. Amaudruz *et al.*, Phys. Rev. Lett. **66** (1991) 2712.

[9] K. Gottfried, Phys. Rev. Lett. **18** (1967) 1174.

[10] A.D. Martin, R.G. Roberts and W.J. Stirling, Phys. Lett. **B252** (1990) 653.

[11] NMC: D. Allasia *et al.*, Phys. Lett. **294B** (1990) 366.

[12] BCDMS collaboration: A.C. Benvenuti *et al.*, Phys. Lett. **223B** (1989) 485.

[13] WA70 collaboration: M. Bonesini *et al.*, Zeit. Phys. **C38** (1988) 371.

[14] EMC: J.J. Aubert *et al.*, Nucl. Phys. **B259** (1985) 189.
K.A. Bazizi, University of California Riverside thesis, 1991.

[15] NMC: P. Amaudruz *et al.*, Nucl. Phys. **B371** (1992) 3.

[16] BCDMS: A.C. Benvenuti *et al.*, Phys. Lett. **237B** (1990) 599.

[17] EMC: J.J. Aubert *et al.*, Nucl. Phys. **B293** (1987) 740.

[18] E605 collaboration: C.N. Brown *et al.*, Phys. Rev. Lett. **63** (1989) 2637.

[19] L.W. Whitlow, E.M. Riordan, S. Dasu, S. Rock and A. Bodek, preprint SLAC-PUB-5442 (1991).

[20] A.D. Martin, W.J. Stirling and R.G. Roberts, Phys. Lett. **B266** (1991) 173.

[21] M. Virchaux and A. Milsztajn, Phys. Lett. **B272** (1992) 221.

[22] T. Hebbeker, review talk at Lepton-Photon Symposium Geneva 1991.

[23] P. Aurenche and M.R. Whalley, Durham-RAL HEP Database, RAL report 89-106 (1989).

[24] L.N. Epele, H. Fanchiotti, C.A. Garcia Canal and R. Sassot, Phys. Lett. **B275** (1992) 155.

[25] B. Badalek and J. Kwiecinski, Nucl. Phys. **B370** (1992) 278.

[26] A.D. Martin, R.G. Roberts and W.J. Stirling, Mod. Phys. Lett. **A4** (1989) 1135.

[27] UA2 collaboration: J. Alitti *et al.*, Phys. Lett. **276B** (1992) 365.

[28] CDF collaboration: F. Abe *et al.*, Phys. Rev. **D44** (1991) 29.

[29] R. Hamberg, W.L. Van Neerven and T. Matsuura, Nucl. Phys. **B359** (1991) 343.

[30] UA2 collaboration: J. Alitti *et al.*, Phys. Lett. **276B** (1992) 354.
CDF collaboration: F. Abe *et al.*, Phys. Rev. **D43** (1991) 2070.

[31] J. Carter, plenary talk at the Joint Lepton-Photon International Europhysics Conference on High Energy Physics, Geneva (1991).

[32] CDF collaboration: F. Abe *et al.*, Phys. Rev. Lett. **64** (1990) 152.

[33] CDF collaboration: F. Abe *et al.*, Phys. Rev. Lett. **68** (1992) 1458.

[34] H. Baer and M.H. Reno, Phys. Rev. **D43** (1991) 2892.

[35] A.D. Martin and W.J. Stirling, Phys. Lett. **248B** (1990) 443.

[36] UA1 collaboration, presented by A. Moulin at the 21st International Symposium on Multiparticle Dynamics, Wuhan, China (1991), Aachen preprint PITHA 91/22 (1991).

[37] A. Moulin, private communication.

[38] A.M. Cooper-Sarkar, G. Ingelman, K.R. Long, R.G. Roberts and D.H. Saxon, Zeit. Phys. **C39** (1988) 281.

[39] E.L. Berger and D. Jones, Phys. Rev. **D23** (1981) 1521.
A.D. Martin, C.-K. Ng and W.J. Stirling, Phys. Lett. **191B** (1987) 200.
NM Collaboration: D. Allasia *et al.*, Phys. Lett. **258B** (1991) 493.

[40] H. Jung, G.A. Schuler and J. Terron, DESY preprint 92-028 (1992).

[41] E.A. Kuraev, L.N. Lipatov and V.S. Fadin, Sov. Phys. JETP **45** (1977) 199.
Ya. Balitsky and L.N. Lipatov, Sov. J. Nucl. Phys. **28** (1978) 822.

[42] A.H. Mueller, Nucl. Phys. B(Proc.Suppl.) **18C** (1990) 125; J. Phys. **G17** (1991) 1443.

[43] J. Bartels, A. De Roeck and M. Loewe, DESY preprint 91-154 (1991).
W.-K. Tang, Columbia preprint CU-TP-532 (1991).
J. Kwiecinski, A.D. Martin and P.J. Sutton, Durham preprint DTP/92/04 (1992).

[44] S.D. Ellis and W.J. Stirling, Phys. Lett. **256B** (1991) 258.

[45] A.D. Martin, W.J. Stirling and R.G. Roberts, Phys. Rev. **D43** (1991) 3648.

Table Captions

1. The upper portion of the table lists the values of the parameters of the parton distributions found in the three types of optimum fit to the data. For sets S_0 and D_0 we fix the gluon exponent $\delta_g = 0$, and for D_- we set $\delta_g = -\frac{1}{2}$. We also list the value of the Gottfried sum rule I_{GSR} and the percentage of the proton's momentum carried by each type of parton at $Q_0^2 = 4$ GeV^2. Finally, we show the values of the K' factor which are required to achieve agreement with the Drell-Yan data of E605[18].

2. Description of the deep inelastic data for the three sets of partons shown in terms of χ^2.

3. Cross sections times leptonic branching ratios for W and Z production at $\sqrt{s} = 630$ GeV and 1.8 TeV. The data are from the UA2 [27] and CDF [28,32] collaborations: the first and second errors are statistical and systematic respectively. The theoretical predictions are described in the text.

Table 1

	S_0	D_0	D_-
$\Lambda_{\overline{MS}}(n_f = 4)$ (MeV)	215	215	215
Glue			
δ_g	0	0	-0.5
γ_g	0	0	12.0
A_g	2.72	2.72	0.315
η_g	5.1	5.1	5.1
Valence			
η_1	0.26	0.45	0.46
η_2	3.82	3.91	3.84
η_3	0.78	0.35	0.24
η_4	4.57	4.66	4.59
ϵ_{ud}	14.4	2.46	3.16
γ_{ud}	16.99	3.32	2.05
ϵ_d	-0.87	11.4	34.4
γ_d	0.82	3.0	9.0
Sea			
η_S	10	10	6.5
A_S	1.87	1.93	0.054
γ_S	6.22	7.38	-3.28
ϵ_S	-2.21	-2.68	19.5
A_Δ	0	0.163	0.144
η_Δ	$-$	0.45	0.46
Drell-Yan K' factor	1.15	1.12	1.09
I_{GSR}	0.333	0.260	0.259
Momentum % at $Q_0^2 = 4$ GeV^2			
Glue	44.6	44.6	44.0
u_{val}	27.6	28.0	28.2
d_{val}	11.7	11.1	10.9
u_{sea}	6.4	5.6	8.0
d_{sea}	6.4	7.3	5.5
s_{sea}	3.2	3.2	3.4

Table 2

Measurement		No. of data	χ^2		
			D_0	S_0	D_-
BCDMS	$F_2^{\mu p}$	142	153	144	148
NMC†	$F_2^{\mu p}$	73	100	101	100
NMC†	$F_2^{\mu D}$	73	78	83	78
EMC	F_2^n/F_2^p	10	3	3	3
BCDMS	F_2^n/F_2^p	11	5	7	5
NMC	F_2^n/F_2^p	11	17	20	17
CDHSW	$F_2^{\nu N}$	84	59	53	60
CDHSW	$xF_3^{\nu N}$	94	53	56	56
CCFR†	$F_2^{\nu N}$	81	36	34	37
CCFR†	$xF_3^{\nu N}$	79	25	30	25

†These data are preliminary and are not yet available in their final form. The errors on the preliminary CCFR measurements have been enlarged to take this into account.

Table 3

	$\sqrt{s}$ (TeV)	$B\sigma_W$ (nb)	$B\sigma_Z$ (pb)	$B\sigma_W/B\sigma_Z$
S_0	0.63	0.768	72.8	10.55
D_0		0.758	73.0	10.39
D_-		0.750	72.8	10.31
B_0		0.752	71.7	10.49
data [UA2]		$0.682 \pm 0.012 \pm 0.040$	$65.6 \pm 4.0 \pm 3.8$	$10.4 \pm^{0.7}_{0.6} \pm 0.3$
S_0	1.8	2.37	222	10.68
D_0		2.37	224	10.61
D_-		2.34	220	10.62
B_0		2.09	200	10.46
data [CDF]		$2.19 \pm 0.04 \pm 0.21$	$209 \pm 13 \pm 17$	$10.2 \pm 0.8 \pm 0.4$

Figure Captions

Fig. 1 The values of $F_2^{\mu p}(x, Q^2)$ as a function of x at $Q^2 = 9$ GeV^2 obtained by interpolating the structure function measurements of the BCDMS collaboration [12] and NMC [4]. The upper curve corresponds to the D_0 set of partons obtained in the present global analysis and the lower curve to the earlier KMRS sets of partons obtained in analyses [7] before the NMC data were available.

Fig. 2 The continuous curves show the description of the BCDMS [12] and NMC [4] measurements of the $F_2^{\mu p}(x, Q^2)$ structure function by the D_0 set of partons. The dashed curves in diagram (a) show the predictions obtained from the KMRS (set B_0) parton distributions [7].

Fig. 3 The description of the BCDMS [12] and NMC [4] measurements of the $F_2^{\mu D}(x, Q^2)$ structure function given by the D_0 set of partons. Sets S_0 and D_- give almost identical fits.

Fig. 4 The description of the NMC data [15] for the structure function ratio $F_2^{\mu n}/F_2^{\mu p}$ given by the D_0, S_0 and D_- sets of parton distributions. The mean Q^2 of the data varies with x as shown by the uppermost scale. The curves take this Q^2 dependence into account.

Fig. 5 The continuous curves show the description of the CDHSW [6] and new preliminary CCFR [5] measurements of the $F_2^{\nu N}(x, Q^2)$ structure function by the D_0 set of partons. All data are shown after correction for the nuclear modification to the structure function. The dashed curves, corresponding to KMRS (set B_0) parton distributions [7], were obtained in an earlier global analysis which included only the CDHSW data.

Fig. 6 As for Fig. 5 but for the structure function $xF_3^{\nu N}(x, Q^2)$.

Fig. 7 Data on the prompt photon transverse momentum distribution in pp collisions at $\sqrt{s} = 23$ GeV from the WA70 collaboration [13] (corrected to $y = 0$ [23]), together with the fit from the D_0 set of partons.

Fig. 8 Parton distributions for the u, d, s quarks and the gluon from the D_0 fit (continuous curves) compared with the earlier B_0 fit [7] (dashed curves).

Fig. 9 The upper curves give the accumulated contribution, $\Sigma(x, 1)$ of eq. (1), to the Gottfried sum rule as a function of x, the lower limit of integration. Predictions are shown for sets S_0, D_0 and D_- of partons. The lower curves compare the integrand, $F_2^{\mu p} - F_2^{\mu n}$, with preliminary estimates by NMC [4].

25

Fig. 10 The behaviour of the sea quark distributions as a function of x for $Q^2 = 10$ GeV^2 and for $Q^2 = 10^4$ GeV^2. The continuous curves correspond to the D$_0$ set of partons (with $\bar{u}$ different from $\bar{d}$) and the dashed curves are for S$_0$ partons (with $\bar{u} = \bar{d}$). For comparison the dot-dashed curves show the $x\bar{u} = x\bar{d}$ distributions of the KMRS(B$_0$) set of partons [7]. The lower two curves show the difference $x\Delta \equiv x(\bar{d} - \bar{u})$ found for the D$_0$ set for $Q^2 = 10$ and 10^4 GeV^2.

Fig. 11 The curve shows $d\log F_2^{\mu N}/d\log Q^2$ calculated from set D$_0$ of partons compared to the values obtained from CDHSW [6] and new preliminary CCFR [5] data.

Fig. 12 The curve shows $d\log F_2^{\mu p}/d\log Q^2$ calculated from set D$_0$ of partons compared to the values obtained from BCDMS [12] and new preliminary NMC [4] data.

Fig. 13 Cross sections times leptonic branching ratios in $p\bar{p}$ collisions as a function of $\sqrt{s}$. The curves are the theoretical predictions calculated to $O(\alpha_s^2)$ in QCD, corresponding to the S$_0$, D$_0$ (continuous)) and D$_-$ (dash-dot) parton distributions. The prediction of set B$_0$ (dotted) of ref.[7] is shown for comparison. The data are from the UA2 [27] (squares) and CDF [28] (circles) collaborations, with statistical and systematic errors added in quadrature.

Fig. 14 As for Fig.13, but for higher collision energies $\sqrt{s}$.

Fig. 15 Rapidity distribution of W^+ bosons produced in $p\bar{p}$ collisions at 1.8 TeV, as predicted by the S$_0$ (dashed), D$_0$ (continuous), D$_-$ (dash-dot) parton distributions to $O(\alpha_s)$. The prediction of set B$_0$ (dotted) of ref.[7] is shown for comparison.

Fig. 16 Charged lepton rapidity asymmetry in $p\bar{p}$ collisions at 1.8 TeV, as predicted by the S$_0$ (dashed), D$_0$ (solid), D$_-$ (dash-dot) parton distributions, in leading order QCD. The prediction of set B$_0$ (dotted) of ref.[7] is shown for comparison. The data are from the CDF collaboration [33], with transverse mass cuts of 50 GeV (solid circles) and 60 GeV (open circle) respectively.

Fig. 17 Rapidity distribution of Z^0 bosons produced in $p\bar{p}$ collisions at 1.8 TeV, as predicted by the S$_0$ (dashed), D$_0$ (continuous), D$_-$ (dash-dot) parton distributions, to $O(\alpha_s)$ in QCD. The prediction of set B$_0$ (dotted) of ref.[7] is shown for comparison.

Fig. 18 The Drell-Yan cross section $M^3 d\sigma/dMdy|_{y=0}$ in $p\bar{p}$ collisions at (a) 630 GeV and (b) 1.8 TeV, as a function of the dilepton mass M. The predictions corresponding to the S$_0$, D$_0$ (continuous), D$_-$ (dash-dot) parton distributions, calculated in $O(\alpha_s)$ QCD, are shown. The prediction of set B$_0$ (dotted) of

26

ref.[7] is shown for comparison. The data are from the UA1 collaboration [36]. The errors are statistical only.

Fig. 19 The structure function $F_2^{\mu p}(= F_2^{ep})$ shown as a function of x at $Q^2 = 20$ GeV^2 for the D$_-$ and D$_0$ set of partons (together with data used in the fits). The dashed curves show the effect of conventional ($R = 5$ GeV^{-1}) and "hot spot" ($R = 2$ GeV^{-1}) shadowing on the D$_-$ prediction. This plot should be compared with Fig. 12 of ref. [7] which gives the extrapolations of $F_2^{\mu p}$ obtained from the KMRS sets of partons.

Fig. 20 Predictions for $F_2^{ep}(x, Q^2) = F_2^{\mu p}(x, Q^2)$ shown as a function of Q^2 for $x = 10^{-1}, 10^{-2}, ...10^{-5}$. The curves correspond to the D$_-$ fit, unshadowed and shadowed with $R = 5$ and $R = 2$ GeV^{-1}.

Fig. 21 The upper and lower sets of curves correspond respectively to the gluon distribution $xg(x, Q^2)$ and the longitudinal structure function $F_L(x, Q^2)$ as functions of x at $Q^2 = 20$ GeV^2. The continuous curves correspond to the D$_-$ and D$_0$ predictions and the dashed curves show the effects of shadowing on the D$_-$ curve.
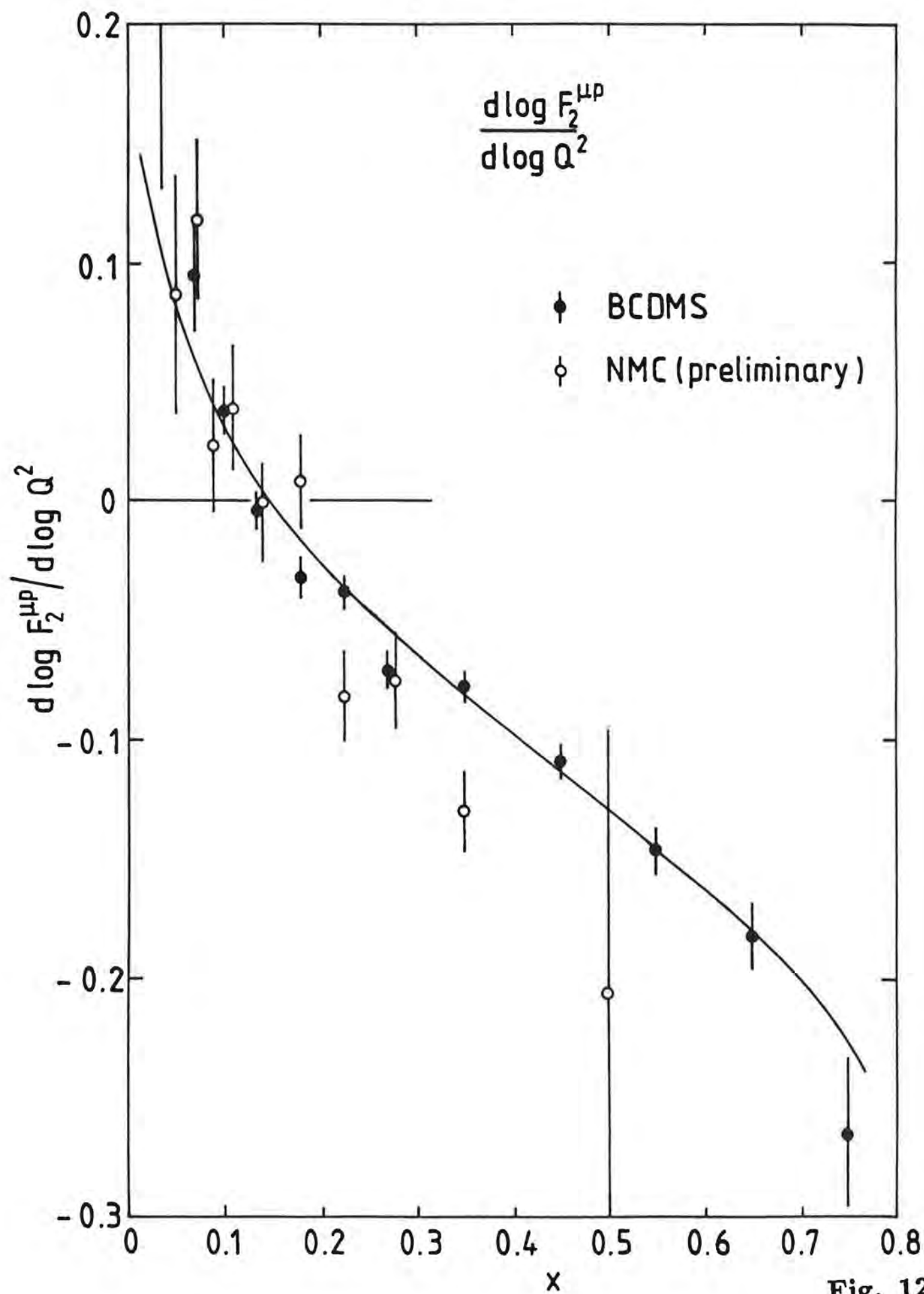
27
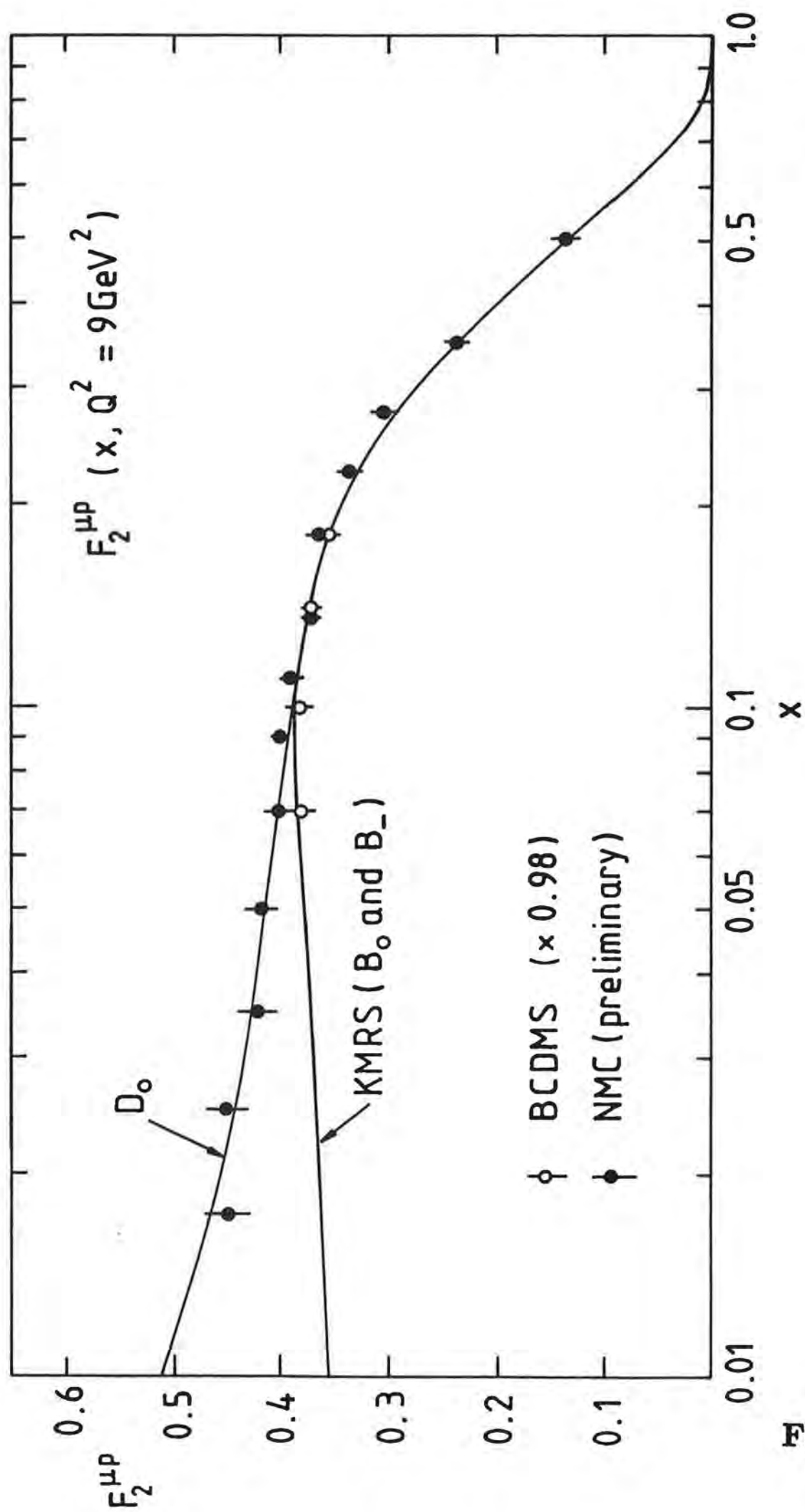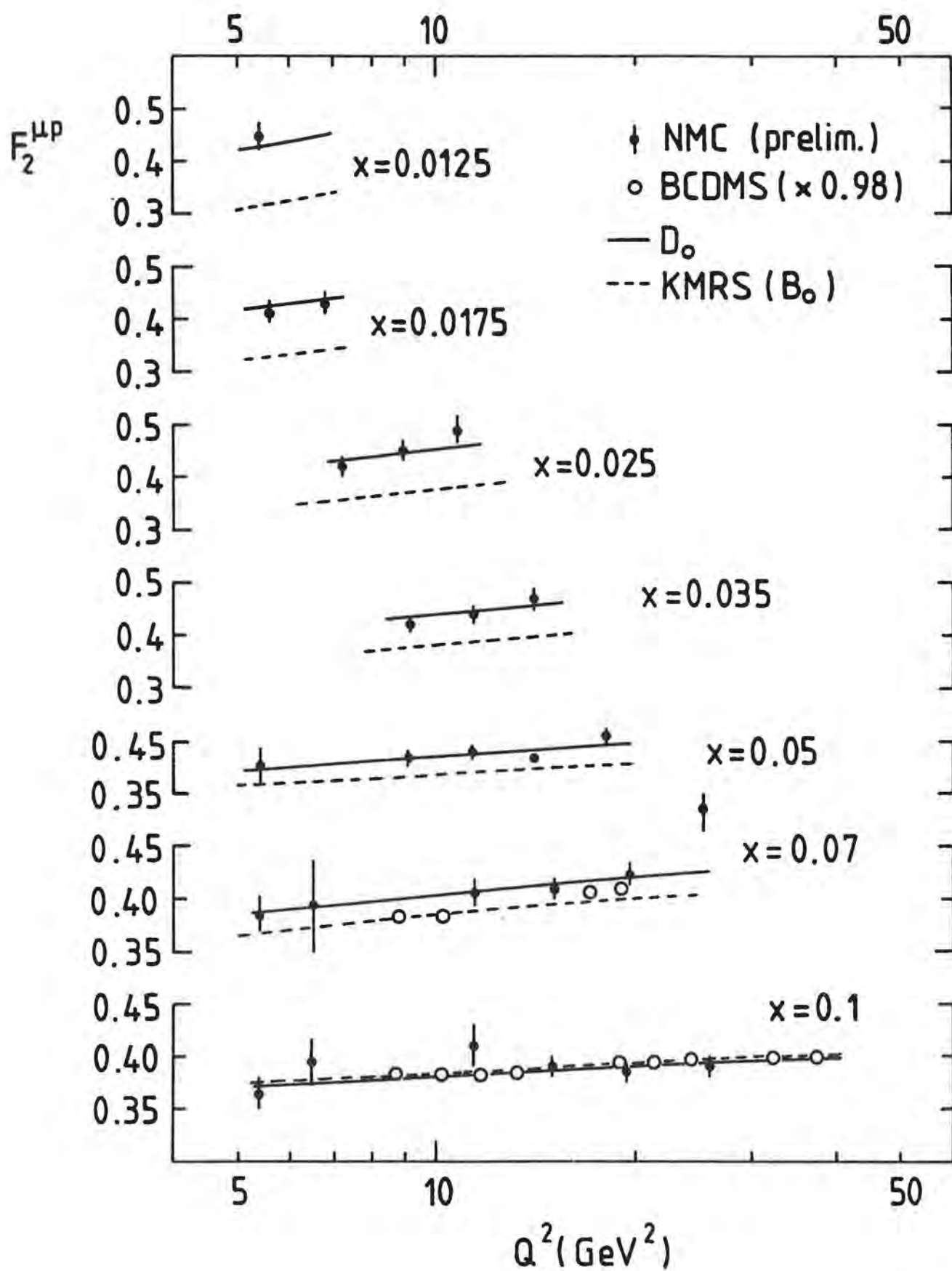
Fig. 1

Fig. 2(a)
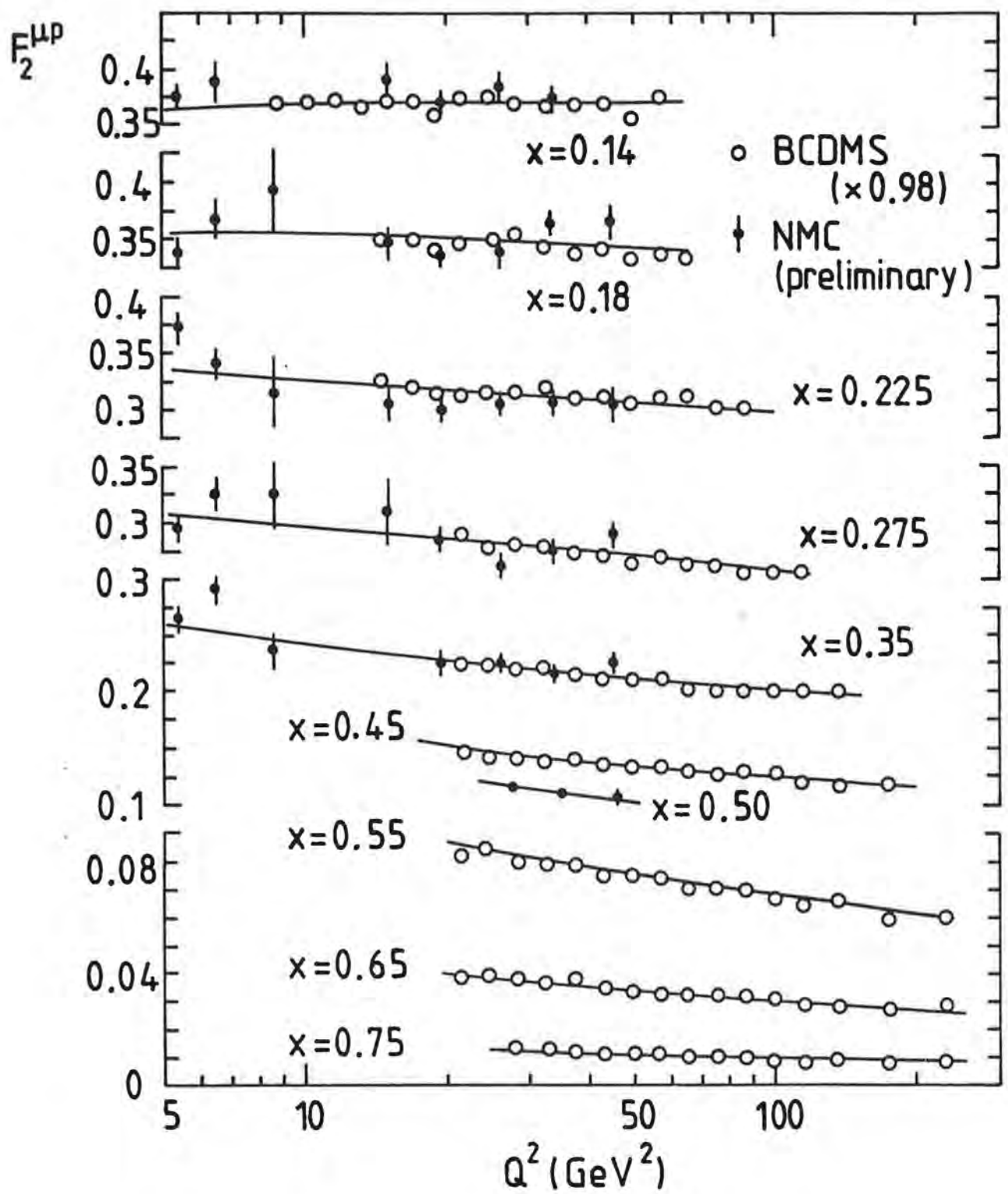
Fig. 2(b)
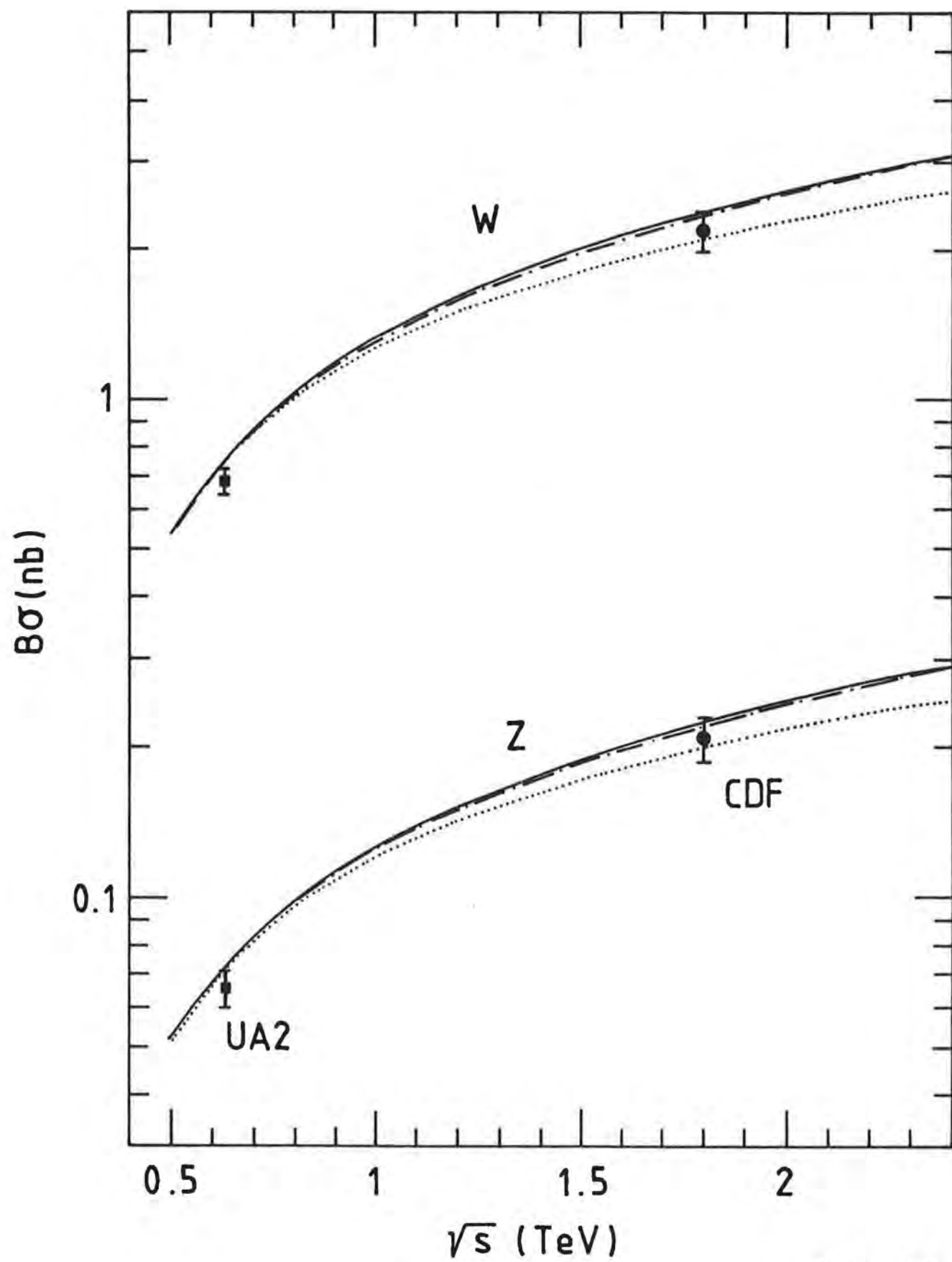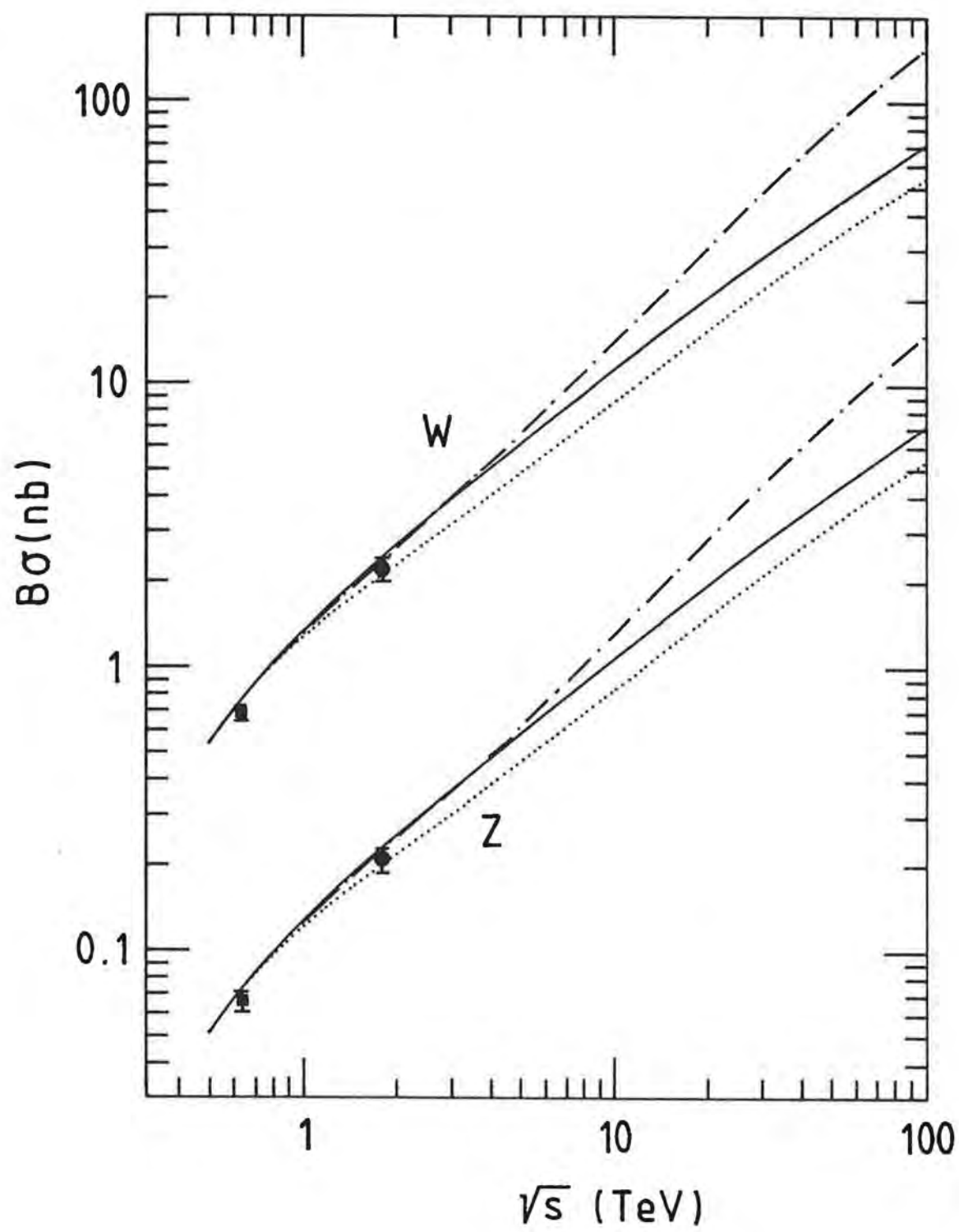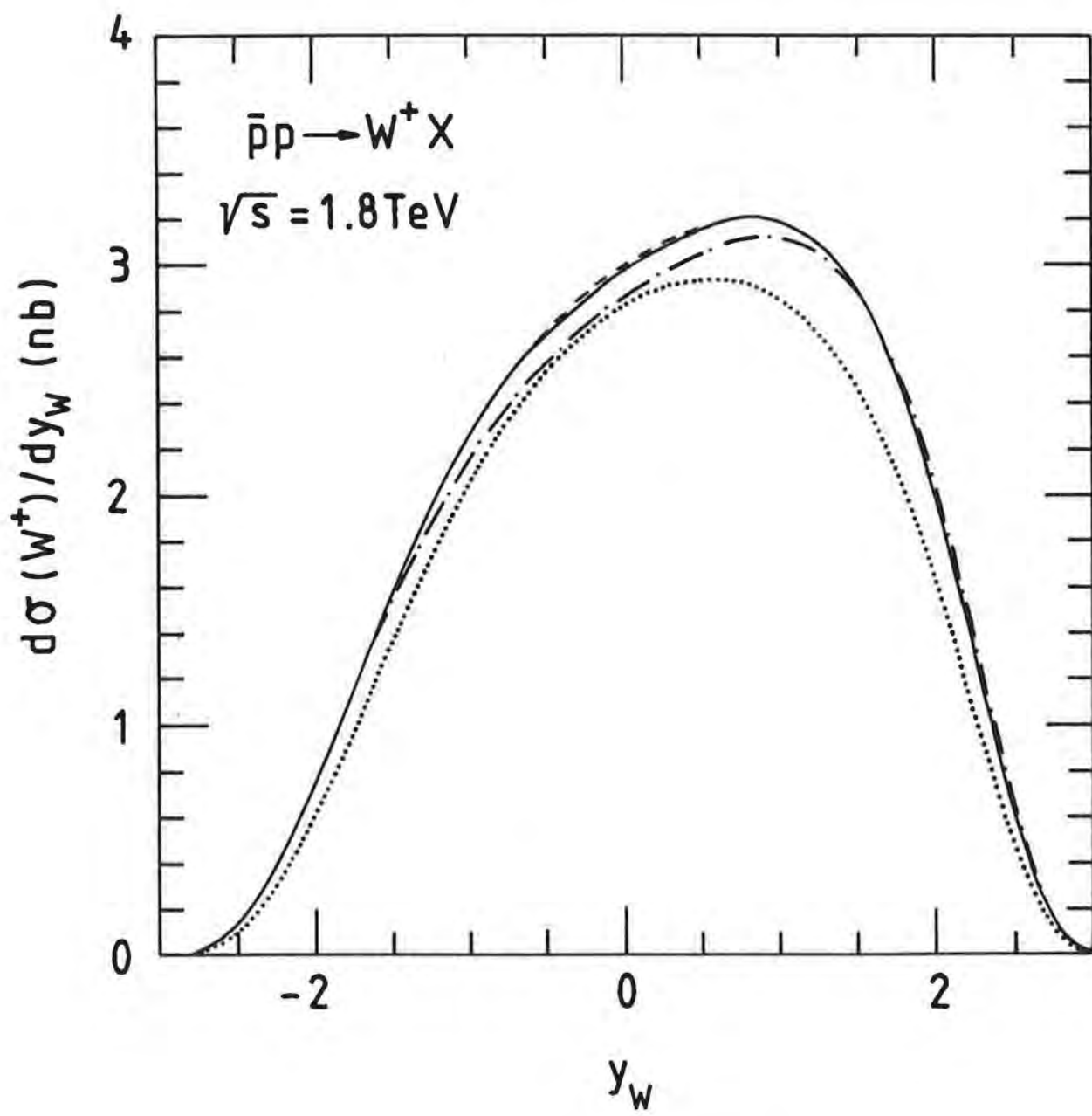
Fig. 3

Fig. 4

Fig. 5

Fig. 6

Fig. 7

Fig. 8

$Q^2 = 20 \, \text{GeV}^2$

D_o

KMRS (B_o)

xu

xd

xs

$xg \, (\times \frac{1}{10})$

$x \, f(x, Q^2)$

x

Fig. 8

$$\int_x^1 \frac{dx'}{x'} \left[F_2^{\mu p}(x') - F_2^{\mu n}(x') \right]$$
at $Q^2 = 7\,\text{GeV}^2$

S_o D_o, D_-

$\frac{1}{3}$

$F_2^{\mu p} - F_2^{\mu n}$ at $Q^2 = 7\,\text{GeV}^2$

S_o

D_-

D_o

ϕ NMC (preliminary)

Fig. 9

Fig. 10

$$\frac{d \log F_2^{\nu N}}{d \log Q^2}$$

● CDHSW

○ CCFR
(preliminary)

Fig. 11

$$\frac{d \log F_2^{\mu p}}{d \log Q^2}$$

● BCDMS

○ NMC (preliminary)

Fig. 12

Fig. 13

Fig. 14

$\bar{p}p \longrightarrow W^+X$

$\sqrt{s} = 1.8\,\text{TeV}$
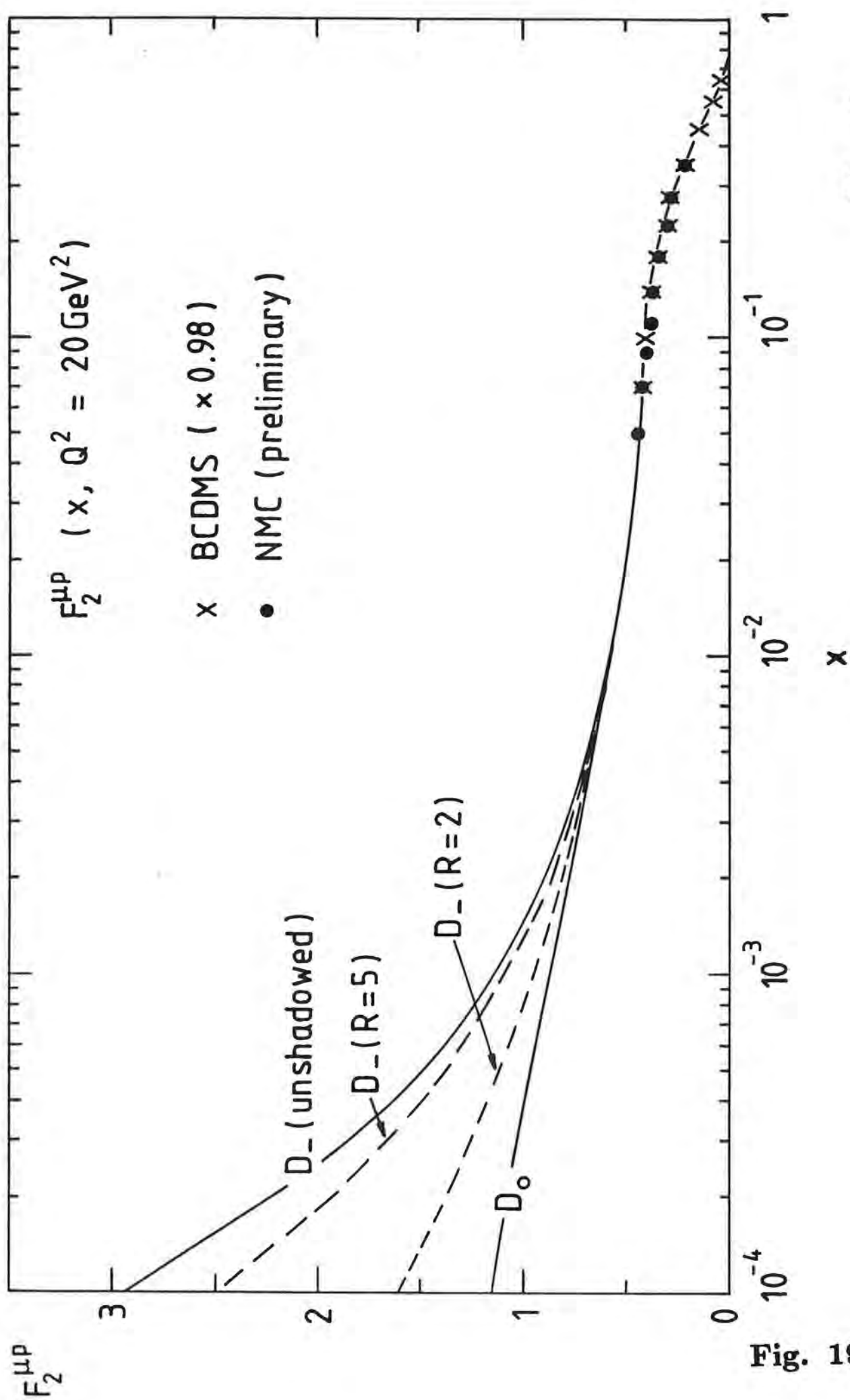
Fig. 15

Fig. 16

$\bar{p}p \longrightarrow ZX$

$\sqrt{s} = 1.8\,\text{TeV}$

Fig. 17

Fig. 18

Fig. 19

Fig. 20

Fig. 21